



Supramolecular nanoassemblies-mediated GSH depletion boosts synergistic chemo- and photodynamic therapy for immunogenicity enhancement

Dun Wang, Wei Ma, Yun Huang, Wei Wang, Shuang Li, Hongbin Liu, Yuqi Zhao, Dongdong Peng, Cui-Yun Yu*, Hua Wei*

Hunan Province Cooperative Innovation Center for Molecular Target New Drug Study, School of Pharmaceutical Science, Hengyang Medical School, University of South China, Hengyang 421001, China

ARTICLE INFO

Keywords:

Supramolecular nanomedicine
GSH depletion
Chemotherapy
Photodynamic therapy
Immunogenicity enhancement

ABSTRACT

O₂-dependent photodynamic therapy (PDT) generally suffers from compromised therapeutic efficiency due to a hypoxic tumor microenvironment. The therapeutic efficiency enhancement of PDT in a hypoxic tumor microenvironment usually requires sophisticated chemical design and multistep preparation and purification procedures. The development of a facile yet robust strategy to improve the therapeutic efficiency of PDT is thus highly desirable for clinical translations, but remains a significant challenge. For this purpose, we reported herein the use of Azobenzene (Azo) not only as conjugation sites for facile construction of multicomponent supramolecular nanomedicine based on a guest homopolymer poly(Azobenzene) (PAzo) and three β-CD-decorated host moieties, *i.e.*, β-CD-modified photosensitizer chlorin e6 (β-CD-Ce6), chemotherapeutic drug cisplatin (β-CD-Pt(IV)), and hydrophilic poly(oligo ethylene glycol) methacrylate (β-CD-POEGMA) via host-guest interactions, but also for glutathione (GSH) depletion-enhanced synergistic chemo- and photodynamic therapy via hypoxia-triggered cleavage of Azo. Notably, the resulting self-assembled supramolecular nanoparticles (NPs) with a Ce6, platinum (IV), and POEGMA molar ratio of 8:8:2 (NP_{Ce6/Pt}) mediated greater cytotoxicity with a half maximal inhibitory concentration (IC₅₀) value 6-fold lower than that of free Ce6 under a hypoxia condition with 660 nm laser irradiation because Azo cleavage-induced GSH depletion boosts synergistic chemo- and photodynamic therapy, which further led to immunogenicity enhancement with a tumor inhibition rate of 93.1% in a murine 4T1 transplantation tumor model. The modularized supramolecular nanoplatform developed herein provides a facile yet robust strategy for advanced combinatory cancer therapy with great potential for clinical translations.

1. Introduction

Photodynamic therapy (PDT) is a highly promising treatment strategy for cancer due to the notable advantages of precise laser controllability, negligible drug resistance, and an excellent tumor-killing effect [1,2]. Basically, photosensitizers (PSs), irradiation laser, and oxygen are the three indispensable ingredients for PDT [3]. Activation of PSs by laser irradiation in the presence of oxygen (O₂) leads to the production of free reactive oxygen species (ROS) including peroxides and singlet oxygen (¹O₂) that further cause tumor cell death [3]. Besides directly eliminating cancer cells, PDT selectively targets the tumor sites and triggers an immunity cell death (ICD) effect by inducing calreticulin (CRT) exposure and releasing high mobility group box 1 (HMGB1) as well as tumor cell fragments [4,5]. However, PDT is insufficient to induce a robust immune response due to the inherent drawbacks of PDT

and an immunosuppressive tumor microenvironment [6]. Hypoxia and high GSH are the typical characteristics of the complex tumor microenvironment (TME) because of the imbalance between the hypoxia suppression of abnormal vascularization and hyperoxia consumption of tumor cells, which greatly compromise the therapeutic efficacy of O₂-dependent PDT [2,7]. Together with PDT-associated further molecular oxygen depletion in the tumor sites, hypoxia exacerbation is thus identified as the substantial reason accounting for PDT treatment failure. Consequently, great efforts have been made in the past decade to improve the PDT treatment efficacy for hypoxic tumors. Although the reported strategies, such as direct delivery of O₂, reduction of tumor O₂ consumption, and compromised abnormal vascular proliferation have shown positive improvements [8–10], most of the methods still suffered from inefficient O₂ generation and too early exposure to O₂, leading to unsatisfactory therapeutic efficiency for clinical translations [11].

* Corresponding authors.

E-mail addresses: yucuiyunusc@hotmail.com (C.-Y. Yu), weih@usc.edu.cn (H. Wei).

<https://doi.org/10.1016/j.cej.2023.143731>

Received 28 March 2023; Received in revised form 6 May 2023; Accepted 22 May 2023
1385-8947/© 20XX

PDT alone is difficult to achieve complete tumor ablation and prevent tumor recurrence. Instead, combinatory therapy holds great promise for overcoming the limited efficiency of monotherapy for cancer treatment. To this end, combinatory PDT and chemotherapy has received considerable attention because of the reported excellent synergistic effects for cancer therapy. On one hand, PDT could restore the immunogenicity of nonimmunogenic chemical drugs by inducing potent immunogenic cell death, which promotes dendritic cell maturation and activates CD8⁺ T cell responses. Additionally, PDT has been shown to improve chemosensitivity of cancer cells, allowing for significantly reduced doses of chemotherapeutic drugs and minimizing the risk of serious side effects on normal tissues [12,13]. Meanwhile, Chemotherapy can not only induce direct cell death through its potent cytotoxicity, but also overcome the disadvantages of PDT, such as oxygen-dependence and limited laser penetration ability, for complementary tumor treatment [14–16]. Therefore, it will be a useful strategy to integrate PDT and chemotherapy for synergistic treatment of hypoxia tumors toward greater efficiency. However, the reported synergistic systems generally required sophisticated chemical design and multistep preparation and purification procedures. The development of a facile yet robust strategy to improve the therapeutic efficiency of PDT is thus highly desirable for clinical translations, but remains a significant challenge.

Host-guest interactions include various non-covalent supramolecular forces, such as charge transfer, electrostatic interactions, hydrophobic interactions, hydrogen bonding, etc, which occur between two components, *i.e.*, the host and guest moieties [17,18]. Cyclodextrins (CDs) are probably one of the most extensively investigated host molecules due to the low toxicity, moderate size, and excellent modifiability. The CD-guest inclusion complex has a modulated binding capacity which provides the possibility to construct diverse stimulatory self-assembly systems that are dynamic and reversible. Trans Azobenzene (Azo) is an ideal guest for the inclusion complexation with cyclodextrin (CD) which is driven by van der Waals and hydrophobic interactions [19]. Unlike other guests of CD with only one triggered sensitivity, the uniqueness of Azo is the multi-sensitivity to a variety of triggers, including laser, hypoxia, and enzymes, which enables broad utilization of Azo for photoisomerization and bioreduction in various biomedical disciplines [20]. The Azo function undergoes intracellular cleavage triggered by GSH or enzyme-mediated bioreductive hypoxia in a hypoxic tumor environment [21,22].

Compared to the recently published notable work [23–25], the main objective of this study is to develop a facile yet robust strategy to improve the therapeutic efficiency of PDT in a hypoxia tumor environment for clinical translations. Inspired by the aforementioned properties of Azo, we reported in this study the use of Azo not only as conjugation sites for facile construction of multicomponent supramolecular nanomedicine based on a guest homopolymer poly(Azobenzene) (PAzo) and three β -CD-decorated host moieties, *i.e.*, β -CD-modified photosensitizer chlorin e6 (β -CD-Ce6), chemotherapeutic drug cisplatin (β -CD-Pt(IV)), and hydrophilic poly(oligo ethylene glycol) methacrylate (β -CD-POEGMA) via host-guest interactions, but also for GSH depletion-enhanced synergistic chemo- and photodynamic therapy via hypoxia-triggered cleavage of Azo. Supramolecular nanoparticles (NPs) were subsequently prepared by the molecular self-assembly of the supramolecular copolymers for synergistic chemo- and photodynamic therapy. The supramolecular NPs undergo tumor accumulation via an enhanced permeation and retention (EPR) effect after intravenous injection. Intracellular Azoreductase and GSH-catalyzed degradation of Azo promotes GSH depletion and disassembly of supramolecular NPs for Ce6 and platinum (IV) release after endocytosis of NPs. Further intracellular reduction of platinum (IV) to cytotoxic platinum (II) species can not only cause a chemotherapeutic effect by directly combining with DNA, but also can enhance the photodynamic effect of Ce6 by activating intracellular nicotinamide adenine dinucleotide phosphate oxidase (NOXs) through multiple pathways to produce superoxide. Mean-

while, the photosensitizer generates cytotoxic ROS under 660 nm illumination, which induces the cells to produce immunogenic death for further triggering a robust immune response to kill tumor cells in conjunction with chemotherapy (Scheme 1). Comprehensive *in vitro* and *in vivo* studies were performed, and an optimized self-assembled supramolecular NP formulation was finally evaluated in a murine 4T1 transplantation tumor model for the immunogenicity enhancement.

2. Methods

2.1. Synthesis of poly (methacrylamido-Azobenzene) (PAzo)

PAzo was prepared by reversible addition and fragmentation chain transfer (RAFT) polymerization using 4-cyanopentanoic acid dithiobenzoate (CPADB) and 2,2'-azobis (2-methylpropionitrile) (AIBN) as a chain transfer agent and an initiator, respectively. CPADB (8.9 mg), methacrylamide-Azobenzene (M-Azo) (0.51 g), and AIBN (1.7 mg) were dissolved in 0.8 mL of dimethylacetamide (DMAc) and the solution was transferred into a Schlenk flask. After the flask was degassed by three freeze-pump-thaw cycles, the reaction mixture was placed at 80 °C for one hour. Then the solution was precipitated in ice anhydrous ether and the precipitate was harvested by centrifugation for three times. Finally, the product was obtained by dried under vacuum.

2.2. Synthesis of CD-Ce6, CD-Pt, and CD-POEGMA

CD-Ce6, CD-Pt, and CD-POEGMA were prepared according to the previously reported procedures.[22,26,27].

2.3. Preparation of NPs

In brief, CD-Ce6, CD-Pt, and CD-POEGMA were dissolved in dimethyl formamide (DMF), and then the organic solutions were added to DMF including PAzo solutions using a syringe pump. After two h of stirring, the NPs were prepared via a classical dialysis method and collected by freeze-drying.

2.4. ROS generation ability

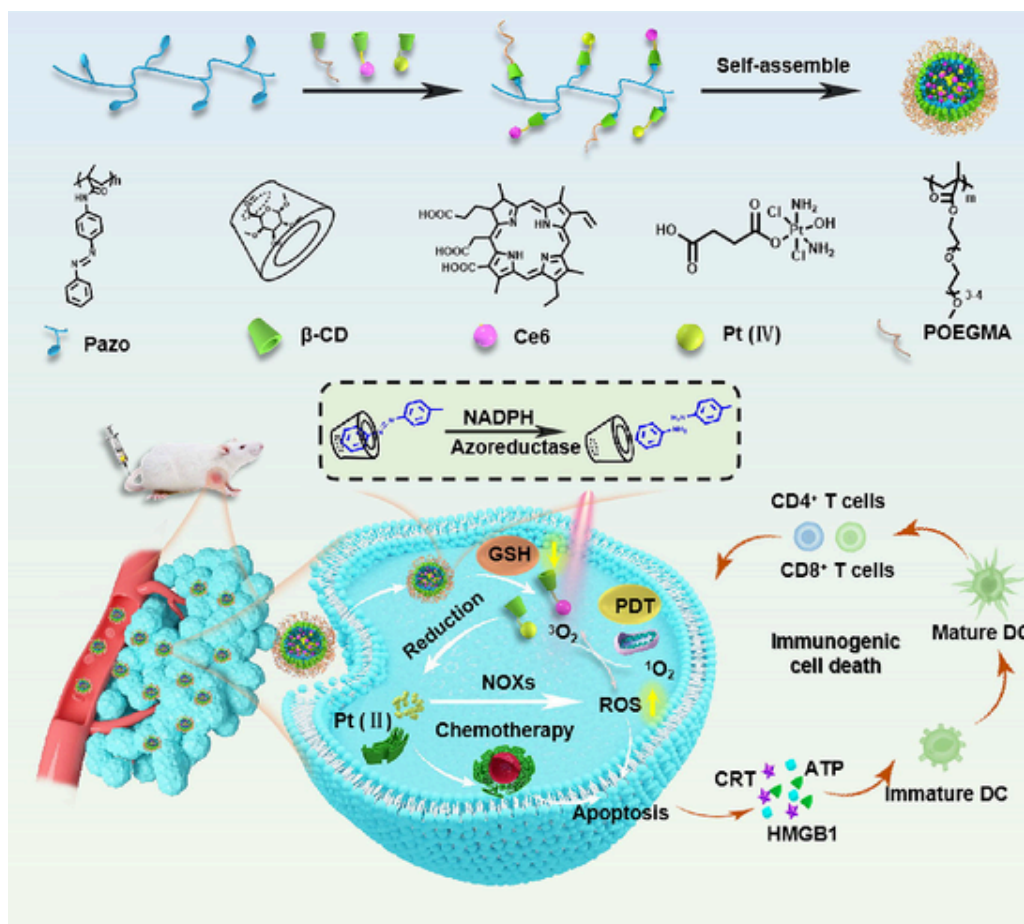
In vitro, the production of ROS by free Ce6 and NP_{Ce6/Pt} was examined by 1,3-diphenylisobenzofuran (DPBF), a classic near-infrared probe. In brief, free Ce6 and NP_{Ce6/Pt} were respectively mixed with DPBF. After that, the mixtures were irradiated in the dark with a 660 nm laser. The rate of ROS production was assessed by the change in fluorescence absorption intensity of the DPBF solution at 415 nm.

2.5. NPs-induced redox imbalance

The GSH level in cells was determined by a Total Glutathione Assay Kit purchase in Beyotime Biotechnology. The cells were cultured in a 4T1 cell-specific medium containing 10 % fetal bovine serum at 37 °C in 5 % CO₂. 4T1 cells (2.0 × 10⁵) were seeded in 12 well plates and cultures for 12 h under either normoxia or hypoxia (5 % O₂, 5 % CO₂ and balanced N₂) environment. Afterward, the cells were incubated with phosphate-buffered saline (PBS) or NP for 2 or 4 h. The cells were collected and mixed with the reagent to rule out the interferences of the protein. The supernatant was collected and further measured according to the assay kit.

2.6. *In vitro* cellular uptake

4T1 cells (1 × 10⁵) were incubated in 24 well plates under normoxia conditions for 24 h. Next, the cells were treated with Ce6 or NP_{Ce6} at an equivalent Ce6 concentration of 5 μ g/mL for 2 or 4 h. After that, the cells were washed three times with PBS to remove the unab-



Scheme 1. Schematic illustration of the synthesis of supramolecular prodrug nanoassemblies and the enhanced immunotherapy via the combination of photodynamic therapy and chemotherapy.

sorbed drugs, followed by fixing them with paraformaldehyde for 5 mins and DAPI for labeling the nucleus. The cells were imaged by a fluorescence inverted microscopy (FIM). For the quantification of fluorescence intensity, the cells were collected after trypsin digestion at the end of the administration and tested by flow cytometry (FCM).

2.7. Live/dead cell staining

4T1 cells were incubated in 24 well plates overnight. The cells were treated with cisplatin (CDDP), Ce6, NP_{Ce6}, NP_{Pt}, and NP_{Pt/Ce6} for 4 h, and the cells in laser groups were irradiated by 660 nm laser for 5 min. Two h later, the cells were washed with PBS and stained by Calcein-AM and PI. FIM was employed to observe the cell survival [28].

2.8. The release of *in vitro* ATP

The cells were seeded in 24 plates under normoxia or hypoxia conditions for 12 h, followed by being treated with different NPs for 6 h. Subsequently, the 4T1 cells were irradiated with a 660 nm laser (0.5 W/cm², 5 min). Then 6 h later, the cells were washed with PBS and lysed by ATP assay lysis solution. The supernatant was collected and examined by an ATP assay kit (Beyotime Biotechnology).

2.9. *In vitro* BMDCs activation and maturation

Primary bone marrow-derived dendritic cells (BMDCs) were isolated from the bone marrow of BALB/c mice. The BMDCs were seeded in 6-well plates and cultured in a medium with GM-CSF and IL-4 for 7 days to acquire immature DCs. Meanwhile, 4T1 cells were treated

with drugs for 4 h and then irradiated for 5 min or not. 12 h later, the immature dendritic cells (DCs) and 4T1 cells were co-cultured for 24 h. Then, BMDCs were collected and stained with CD11c, CD86, and CD80 for 30 min. The results were measured by FCM.

2.10. *In vivo* immune activation

To verify the immune effect of NPs *In vivo*, we established 4T1 transplanted tumor mouse model. After being treated 3 times according to the steps of tumor suppression experiments, mice were executed to collect spleen and tumor tissues for digestion and cell collection. To detect DC cell maturation rates, cells collected from the spleen and tumor tissues were incubated with anti-CD86, anti-CD80, and anti-CD11c. To determine the ratio of CD8⁺CD4⁺T cells, spleen cells were incubated with anti-CD4, anti-CD8, and anti-CD3. Tumors were collected and subjected to immunofluorescence staining.

2.11. *In vivo* biosafety study

The blood of each mouse was collected on day 15. The samples were kept for 2 h and the serum of each sample was collected through centrifugation. The serum samples were analyzed by Wuhan Xavier Biotechnology Co for alanine aminotransferase (ALT), aspartate aminotransferase (AST), blood urea nitrogen (BUN), creatinine (Cr), creatine kinase (CK), and lactate dehydrogenase (LDH). Tumors and major organs were excised and subjected to H&E staining and immunofluorescence staining.

3. Results and discussion

3.1. Synthesis and characterization of supramolecular copolymers and formation of nano-assemblies

The synthesis procedures of supramolecular copolymers were schematically illustrated in Fig. S1. Briefly, a methacrylamide monomer bearing azobenzene moiety (denoted as M-Azo) was synthesized by amidation coupling (Fig. S1A), whose structure was confirmed by ^1H NMR spectrum (Fig. S2). Then the guest polymers containing azobenzene (denoted as PAzo) were prepared by reversible addition and fragmentation chain transfer (RAFT) polymerization of M-Azo using 4-cyanopentanoic acid dithiobenzoate (CPADB) as a chain transfer agent (CTA). The representative chemical structure of PAzo was verified by ^1H NMR (Fig. S3A) and size-exclusion chromatography (SEC) (Fig. S3B). The degree of polymerization (DP) of PAzo was calculated by monomer conversion and modulated by the control of the polymerization time confirmed by clearly increased molecular weight (MW) with extended polymerization time (Table S1). The unimodal and narrow-distributed SEC elution traces with low polydispersity index ($PDI < 1.2$) of three PAzo suggest the well control toward MWs and MW distribution.

Three different host β -CD units containing poly (oligo ethylene glycol) methacrylate (POEGMA), chlorine e6 (Ce6), and cisplatin (Pt(IV)) were prepared according to the previously reported procedures, which were denoted as β -CD-POEGMA, β -CD-Ce6, and β -CD-Pt, respectively (Fig. S1). [26,27,29] Among, β -CD-POEGMA was used as a hydrophilic host moiety of the nano-assemblies for improved colloid stability, which was prepared by click coupling between azide-decorated β -CD (β -CD- N_3) and alkyne-terminated POEGMA (POEGMA-alkyne) (Figs S1B and S4-S6). The successful synthesis of β -CD-POEGMA is confirmed by the appearance of all the typical signals attributed to β -CD and POEGMA as well as the presence of a resonance signal peak at 8.05 ppm assigned to the triazole function formed after click coupling in the ^1H NMR spectrum of β -CD-POEGMA (Fig. S6). Two anticancer host prodrugs β -CD-Ce6 and β -CD-Pt were prepared by conjugating Ce6 and Pt(IV) to β -CD via amidation coupling, respectively (Fig. S1C and D). The equivalent coupling between β -CD and Ce6/Pt was supported by the ^1H NMR data (Figs. S7 and S8).

Facile mixing of hydrophobic guest PAzo and hydrophilic host β -CD-POEGMA with different molar ratios resulted in self-assembled micelles

with for optimizing nanoparticle sizes (Table S2). The nanoparticle with 1:2 M ratio of PAzo to β -CD-POEGMA (denoted as NP) was selected as the optimized one with smaller particle size relative to that of the other two nanoparticles with 1:1 and 3:1 M ratio. Subsequent mixing of NP, β -CD-Ce6, and β -CD-Pt at an optimized molar feed ratio of 1:2:8:8 led to the formation of stabilized nanoparticles (denoted as $\text{NP}_{\text{Ce6/Pt}}$) with a smaller average diameter of approximately 150 nm due to the hydrophilic/hydrophobic balance of the whole supramolecular systems (Table S3 and Fig. 1A). Meanwhile, the hydrodynamic diameters of the NP containing only Ce6 (denoted as NP_{Ce6}) or Pt(IV) (denoted as NP_{Pt}) were determined by dynamic laser scattering (DLS) to be 136 nm and 125 nm, respectively (Fig. S9). The excellent salt stability of $\text{NP}_{\text{Ce6/Pt}}$ was evidenced by the uniform sizes and size distributions in phosphate-buffered saline (PBS) without any significant changes in 7 days (Fig. 1B). Both NP_{Ce6} and $\text{NP}_{\text{Ce6/Pt}}$ share an identical ultraviolet-visible (UV-Vis) characteristic adsorption band ascribed to the free Ce6, supporting the successful incorporation of Ce6 in the self-assembled NPs (Fig. 1C). The loading contents of Ce6 and Pt in $\text{NP}_{\text{Ce6/Pt}}$ were calculated to be 7.56 % and 6.02 % based on the quantitative analysis of UV-Vis spectra and inductively coupled plasma (ICP) results, respectively. Taken together, $\text{NP}_{\text{Ce6/Pt}}$ fabricated via readily mixing of four different supramolecular moieties showed excellent colloidal stability and desired loading amounts of therapeutic agents for controlled release applications.

The Azo moiety in $\text{NP}_{\text{Ce6/Pt}}$ can be cleaved intracellularly by the overexpressed azoreductase and GSH in a hypoxia tumor environment [22]. To investigate the hypoxia-sensitivity of $\text{NP}_{\text{Ce6/Pt}}$ in vitro, $\text{NP}_{\text{Ce6/Pt}}$ was treated with sodium dithionite ($\text{Na}_2\text{S}_2\text{O}_4$), an important hypoxia biomarker, which led to significantly compromised intensity of the typical UV absorption band of Azo centered at 350 nm due to hypoxia-induced dissociation of Azo (Fig. 1D). The azoreductase-triggered cleavage of Azo was strongly supported by the size distribution and morphology changes of $\text{NP}_{\text{Ce6/Pt}}$ under a reduction-mimicking condition with 10 mM $\text{Na}_2\text{S}_2\text{O}_4$ which reveals bimodal size populations with a quite broad distribution (Fig. S10A) and formation of large aggregates with irregular morphologies (Fig. S10B). [11,30,31] On the other hand, the inert Pt(IV) prodrug in $\text{NP}_{\text{Ce6/Pt}}$ undergoes intracellular GSH or ascorbic acid (ASA)-triggered reduction to Pt(II) for the exertion of cytotoxicity on cancer cells [29]. Therefore, incubation of $\text{NP}_{\text{Ce6/Pt}}$ with 10 mM ASA that mimics the intracellular reductive environment promoted a dramatic increase of Pt(II) release to 65 % in 48 h in contrast to

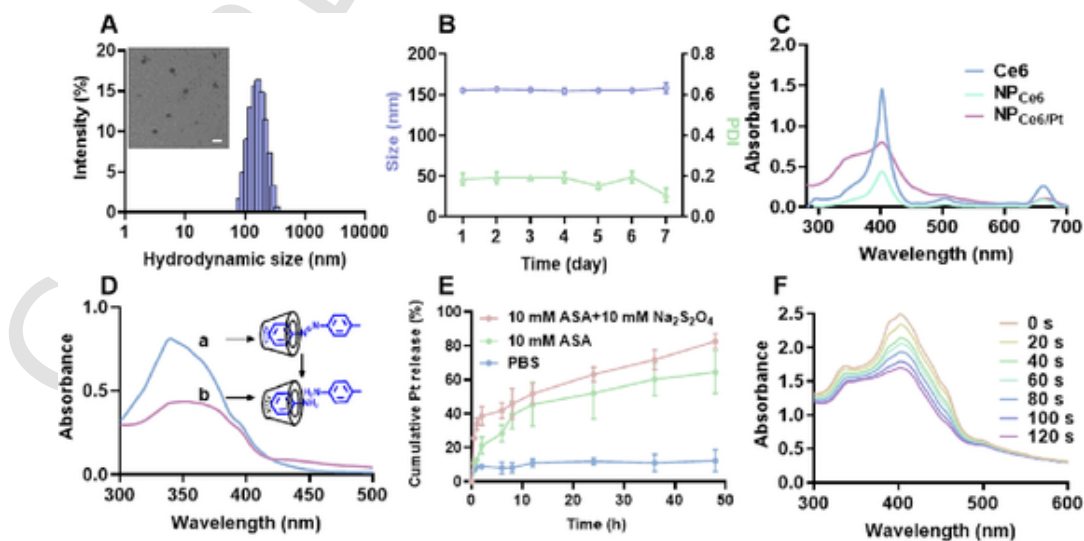


Fig. 1. Physicochemical characterization of supramolecular prodrug nanoparticles. (A) TEM images and size distributions of $\text{NP}_{\text{Ce6/Pt}}$. PDI = 0.12. Scale bar: 200 μm . (B) Particle size change of $\text{NP}_{\text{Ce6/Pt}}$ in PBS, ($n = 3$). (C) UV-vis spectra of Ce6, NP_{Ce6} , and $\text{NP}_{\text{Ce6/Pt}}$. (D) Absorption spectra of the Azo/ β -CD complex solution under a) normoxia and b) hypoxia conditions. (E) In vitro Pt release profiles from $\text{NP}_{\text{Ce6/Pt}}$ under different conditions. (F) Time-dependent UV absorption spectra of DPBF in $\text{NP}_{\text{Ce6/Pt}}$ after irradiation with a 660 nm laser (0.5 W/cm^2).

negligible Pt release in the absence of ASA (Fig. 1E). The incomplete cumulative drug release less than < 80 % in the presence of ASA was likely attributed to the steric hindrance of hydrophilic POEGMA chains, which prevents the loaded cargoes from complete out diffusion in 48 h [32,33]. However, the cumulative drug release significantly increased to 83 % in hypoxic and reducing conditions (added in Fig. 1E as suggested), which is reasonably ascribed to the hypoxia-triggered cleavage of Azo for nanoparticulate destruction and promoted Pt (IV) reduction and release [34–37]. The results confirm that the excellent extracellular colloidal stability of NP_{Ce6/Pt} with minimal Pt(II) leakage and accelerated intracellular Pt(II) release triggered by the tumor microenvironment.

Next, the ROS generation ability of NP_{Ce6/Pt} was determined by using a ¹O₂ indicator fluorescence probe DPBF. Due to DPBF can react with ROS to quench its UV absorption peak at 415 nm, and the degree of quenching is positively correlated with the ROS concentration in the environment [38]. A mixture of NP_{Ce6/Pt} and DPBF was subjected to 660 nm laser irradiation for 2 min followed by the recording of UV changes at different time points. It is worth pointing out that Ce6 and NP_{Ce6/Pt} show quite similar ROS generation properties, implying any insignificant effects of modification and synthesis on the photodynamic properties of Ce6 (Fig. 1F and Fig. S11).

3.2. In vitro cellular uptake and cytotoxicity

The maintenance of a dynamic balance between GSH and ROS plays an important role in regulating oxidative stress of tumor cells [39]. The intracellular dissociation of Azo leads to GSH depletion that further

boosts synergistic chemotherapy and PDT. The intracellular GSH levels of 4T1 cells after different treatments were quantified by a total glutathione assay kit. Interestingly, incubation with NP_{Ce6/Pt} led to significantly decreased intracellular GSH level under hypoxia conditions in contrast to a negligible effect on GSH level under normoxia conditions likely due to the reduction and breakage of Azo by intracellular nicotinamide adenine dinucleotide phosphate hydrogen and azoreductase (Fig. 2A) [19,22,40]. The cellular uptake efficiency of free Ce6 and NP_{Ce6/Pt} was evaluated by a fluorescence inverted microscopy (FIM) and flow cytometry (FCM) in 4T1 cells. The Ce6 fluorescence was used for quantification via FCM. NP_{Ce6}-treated 4T1 cells show a mean fluorescence intensity (MFI) 3.5-fold greater than that of free Ce6-incubated cells after 4 h of incubation likely due to the improved solubility of Ce6 in a particulate-based formulation (Fig. 2B). Similar results were observed by fluorescence inverted microscopy, which reveals much greater red fluorescence intensity in NP_{Ce6}-treated 4T1 cells than that of free Ce6-incubated cells (Fig. 2C). To evaluate the ROS generation ability of PDT for killing cancerous cells, the intracellular ROS level produced by NP_{Ce6/Pt} under laser irradiation was detected by a ROS indicator, 2,7-dichlorofluorescein diacetate (DCFH-DA) that can produce green fluorescence after being oxidized by ROS (Fig. 2D). Interestingly, NP_{Ce6/Pt} could lead to a weak fluorescence without laser due to the Pt(II) release-activated intracellular NOXs for ROS production [37]. The cells treated with free Ce6, NP_{Ce6}, or NP_{Ce6/Pt} showed bright green fluorescence under laser irradiation and normoxia condition. Note that hypoxia significantly attenuates the ROS generation efficiency of free Ce6 compared to a normoxia condition as O₂ is one of the most important agents for triggering PDT. Most importantly, the cells treated with

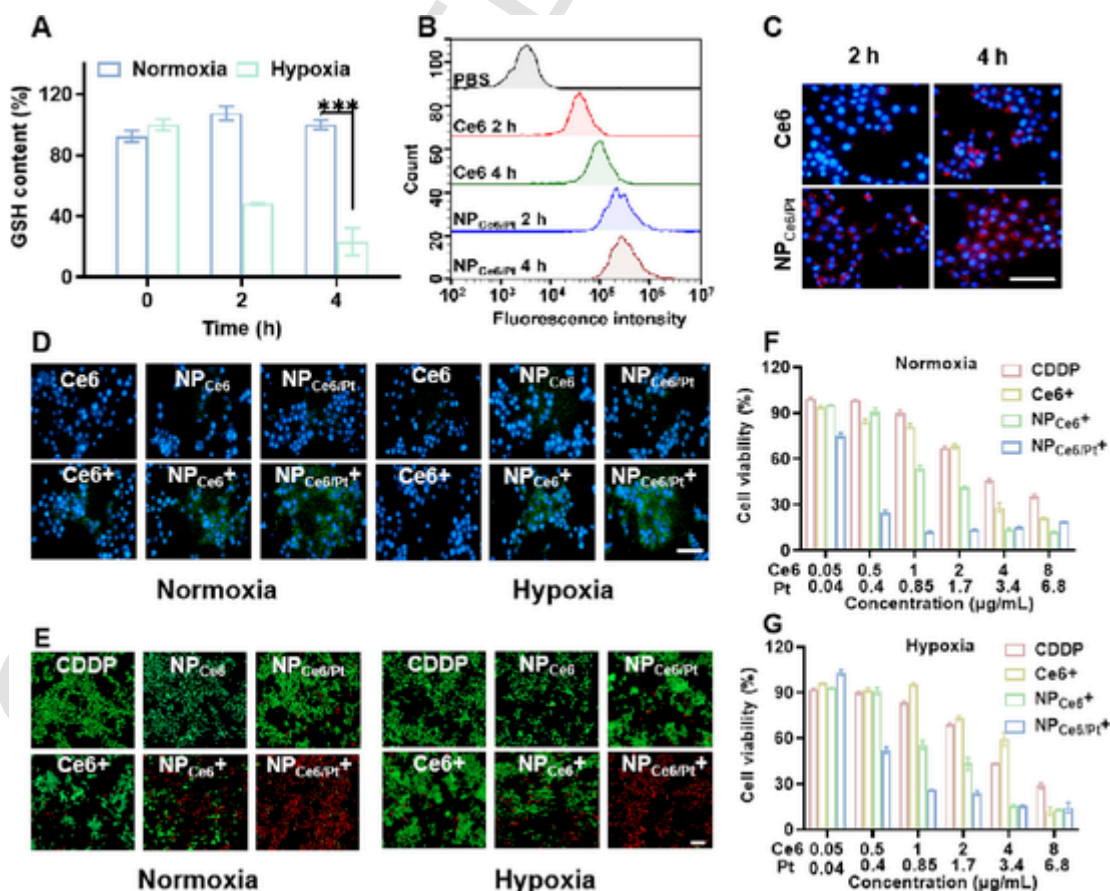


Fig. 2. In vitro evaluation of the anticancer. (A) Relative intracellular GSH level under normoxia and hypoxia conditions. (B) Fluorescence intensity of 4T1 cells cultured with free Ce6 or NP_{Ce6/Pt}. (C) Images of 4T1 cells incubated with free Ce6 or NP_{Ce6/Pt} for 2 h and 4 h. Scale bars: 100 µm. (D) FIM images of 4T1 cells were treated with different samples and subsequently stained by DCFH-DA. Scale bar: 100 µm. (E) Calcein AM and PI staining of 4T1 cells after administration of the treatment. Scale bar: 200 µm. Cell viabilities of 4T1 cells treated with various NPs under normoxia (F) and hypoxia conditions (G) for 24 h.

NP_{Ce6/Pt} + show quite similar fluorescence intensities with negligible differences between normoxia and hypoxic conditions, indicating the capability of NP_{Ce6/Pt} to overcome the disadvantage of O₂-dependent PDT. The cytotoxicity of Ce6 can only be activated when laser irradiation is applied. To evaluate the cytotoxicity of various formulations, 4T1 cells were incubated with different formulations at various concentration gradients for MTT assay. Free Ce6 and NP_{Ce6} did not induce significant toxicity to cells in the absence of laser treatment even at Ce6 doses up to 20 µg/mL, supporting the excellent biocompatibility of Ce6 and NP_{Ce6} (Fig. S12). A 660 nm laser irradiation at 0.5 W/cm² for 5 min led to a clear inhibitory effect on the cell proliferation with the half maximal inhibitory concentration (IC₅₀) values of 2.71, 1.40, and 0.16 µg/mL for free Ce6, NP_{Ce6}, and NP_{Ce6/Pt}, respectively (Fig. 2F). The higher cytotoxicity of NP_{Ce6} than that of free Ce6 is relative to the greater cellular uptake efficiency and ROS production capacity of NP_{Ce6}. Promisingly, NP_{Ce6/Pt} shows an IC₅₀ value 7-fold lower than that of free Ce6 under a hypoxia condition owing to the Azo units of NP_{Ce6/Pt}-induced GSH depletion for enhanced chemotherapy and PDT with greater synergistic therapeutic efficiency (Fig. 2G). NP_{Ce6/Pt} show comparable IC₅₀ values for 4T1 and MCF-7 cells and similar dose-dependent inhibitory effects, suggesting the broad-spectrum anticancer properties of the reported nanoparticles (Fig. S13 and Table S4). The same phenomenon is observed by the fluorescence microscope-based vivid live/dead cell staining assay with live cells stained in green fluorescence and dead ones in red fluorescence (Fig. 2E).

3.3. In vitro immune response study

PDT has been revealed to be a highly potent immunity cell death (ICD) inducer for triggering immune response for enhanced immunogenicity of tumors after killing cells.[41,42] calreticulin (CRT) expression, high mobility group box 1 (HMGB1) release, and adenosine

triphosphate (ATP) secretion were measured to assess the efficacy of immune response by NP_{Ce6/Pt}. 4T1 cells after various treatments were subjected to immunofluorescence staining to observe CRT exposure and HMGB1 release. CRT was expressed on the surface of apoptotic tumor cells during ICD, which provides an “eat-me” signal for antigen-presenting cells. The expression of CRT on the cell surface was observed by FIM (Fig. 3A). Faint green fluorescence is observed in the cells treated with CDDP and NP_{Pt} due to cisplatin-induced immunologically silent cell death without any CRT translocation to the cell surface. Exposure to laser irradiation led to significantly increased green fluorescence of 4T1 cells treated with Ce6, NP_{Ce6}, or NP_{Ce6/Pt}, which indicates high CRT expression. Further quantification of single-cell fluorescence intensity shows a CRT green fluorescence expression 1.8-fold higher after NP_{Ce6} + treatment than that of Ce6 + (Fig. 3B and Fig. S14). Notably, NP_{Ce6/Pt} + efficiently promoted the CRT-positive rate of 4T1 cells to 77.22 %, 3.5-fold greater than that of Ce6 +, strongly supporting the superior ICD induction ability of synergistic chemotherapy-PDT strategy in vitro. The HMGB1 release was next measured by immunostaining analysis as well (Fig. 3C). The negligible green fluorescence of HMGB1 in the NP_{Ce6/Pt} + group confirms the HMGB1 escape from the tumor cells. A decrease of the co-localization coefficient from 0.99 to 0.60 further confirms the anti-tumor ability of NP_{Ce6/Pt} + (Fig. 3D and Fig. S15). To finally validate the ICD effect, the ATP secretion was assessed by an ATP assay kit. The amount of ATP secreted in the NP_{Ce6/Pt} + treated cells is nearly 4-fold higher than that of the PBS control. The NP_{Ce6/Pt} + treated group secretes ATP 28 % more than Ce6 + treated group under a hypoxia condition (Fig. 3E and F). Collectively, the results on CRT exposure, HMGB1 release, and ATP secretion all confirm a greater ICD effect as a result of synergistic cisplatin-mediated chemotherapy and photosensitizer Ce6-mediated PDT.

After confirming the ICD-inducing properties of NP_{Ce6/Pt}, we further evaluated the maturation of dendritic cells (DCs) in vitro (Fig. 3G and

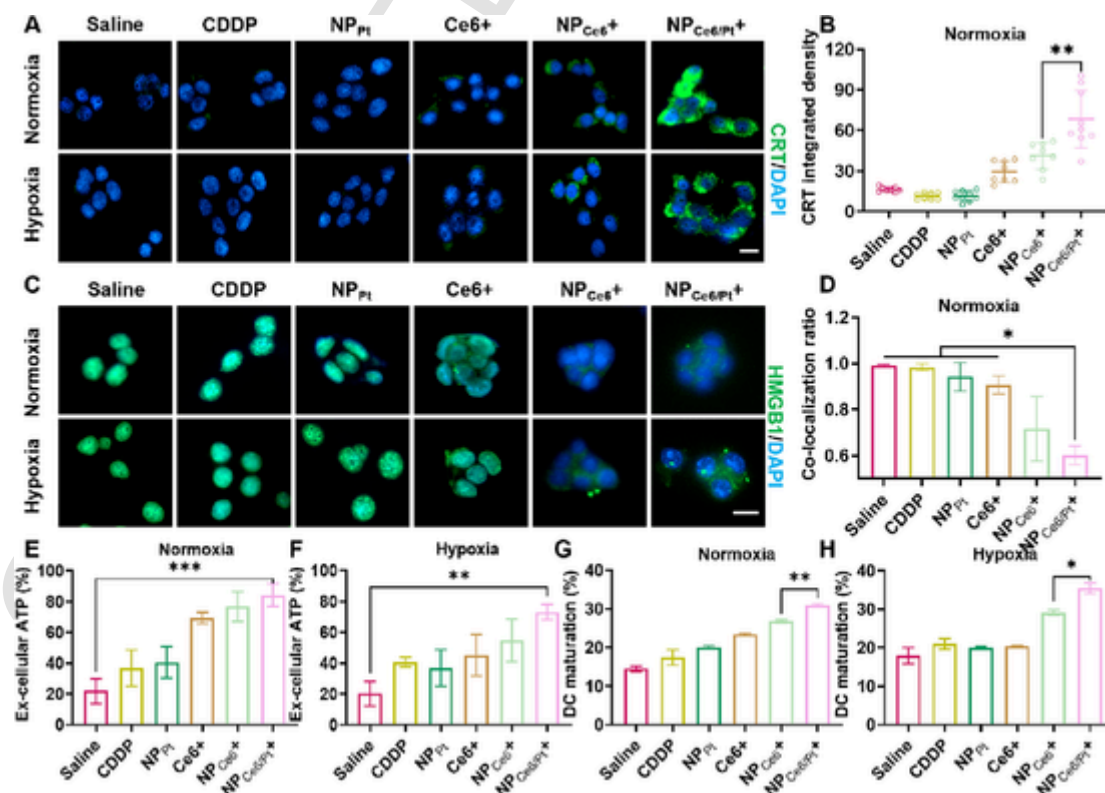


Fig. 3. In vivo anti-tumor immune response. (A) The images of 4T1 cells treated with different treatments for CRT measure. Scale bar: 20 µm. (B) Quantification of CRT exposure under normoxia by single cell fluorescence intensity. (C) The images of 4T1 cells with treated with different treatments for HMGB1 measure. Scale bar: 20 µm. (D) Co-localization coefficients between HMGB1 and nuclei in 4T1 cells under normoxia. (E) Quantification of ATP secretion in the supernatant of 4T1 cells under normoxia (E) and hypoxia (F) conditions. Maturation of DCs quantified by flow cytometry under normoxia (G) and hypoxia (H) conditions.

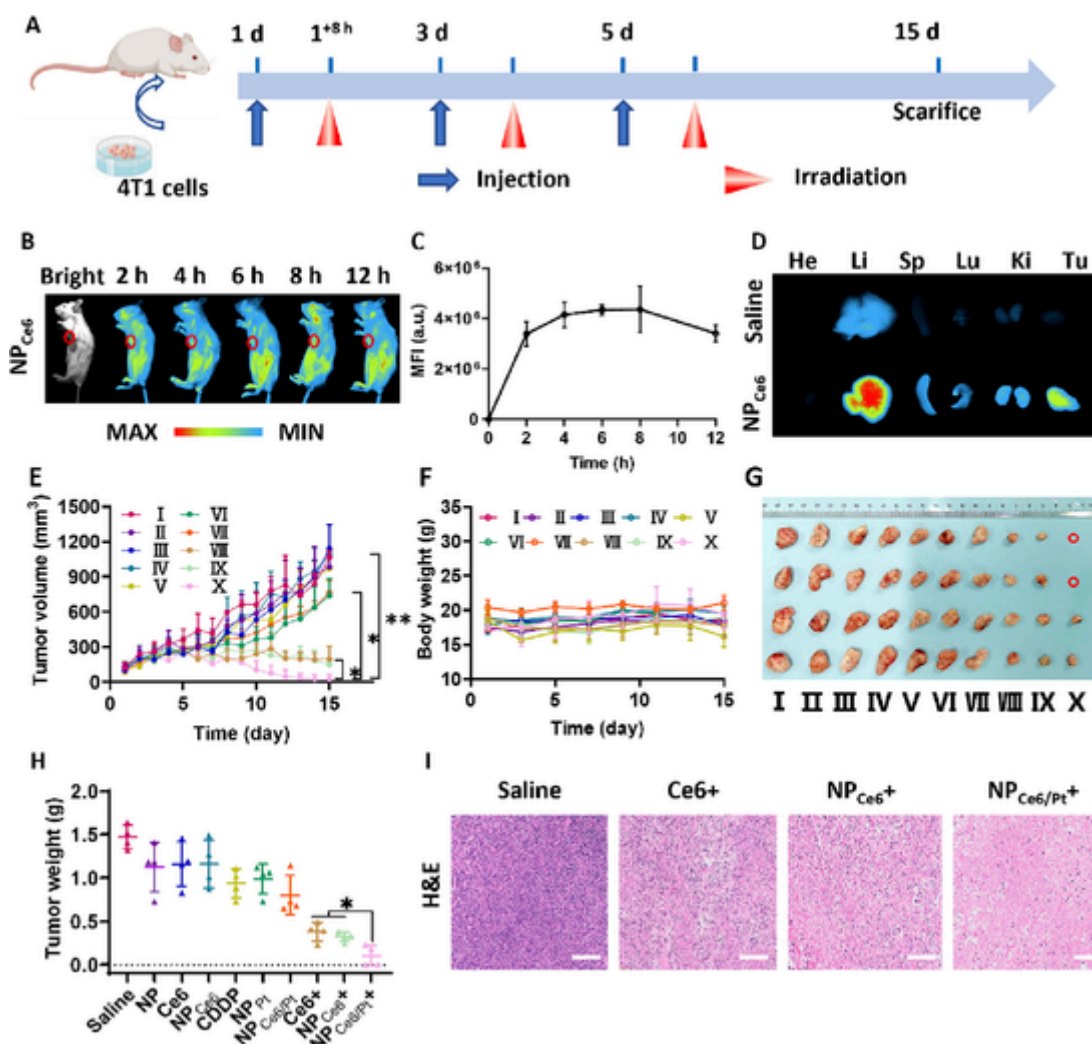


Fig. 4. *In vivo* therapeutic efficacy. (A) Schematic illustration of the PDT treatment strategy. (B) *In vivo* fluorescence images of 4T1 bearing mice after intravenous injection with NP_{Ce6} at different time points. (C) Time-dependent mean fluorescence intensity of tumor sites. (D) The ex vivo fluorescence images of the tumor and major organs from the NP_{Ce6}-treated mice at 12 h post-injection. He, heart; Li, liver; Sp, spleen; Lu, lung; Ki, kidney; and Tu, tumor. (E) The tumor growth curves and body weight change (F) in different groups. I: Saline; II: NP; III: Ce6; IV: NP_{Ce6}; V: CDDP; VI: NP_{Pt}; VII: NP_{Ce6/Pt}; VIII: Ce6 +; IX: NP_{Ce6} +; X: NP_{Ce6/Pt} +. (G) Photographs of tumors extracted from mice with different treatments. (H) The tumor weights after the entire antitumor study. (I) The H&E staining images of tumor tissues after administration for 15 days. Scar bar: 200 μ m.

H). The number of mature DCs significantly increases in the NP_{Ce6/Pt} + group relative to the control group, which is consistent with the results of damage-associated molecular patterns (DAMPs) release. Notably, the maturation rate of the DCs co-cultured with NP_{Ce6/Pt} + under an anoxic condition reached 35 %, two-fold greater than those of the groups treated with Saline, CDDP, NP_{Pt}, and Ce6 +. Therefore, NP_{Ce6/Pt}-mediated combined treatment under laser irradiation can cause CRT translocation to the cell surface and promote the extracellular HMGB1 and ATP release for enhanced anti-tumor immunity with ICD inducing and DC maturation.

3.4. *In vivo* biodistribution and antitumor efficacy study

In this study, 4T1 cells subcutaneous tumor-bearing mouse model were used to evaluate the anti-tumor effect of self-assembled nanoparticles based on synergistic chemo- and photodynamic therapy (Fig. 4A). The biodistribution of NP_{Ce6} in 4T1 tumor-bearing mice was investigated by fluorescence inverted microscopy prior to *In vivo* antitumor activity study. The results confirmed sustained accumulation of NP_{Ce6} at the tumor site likely due to the accumulation ability of NPs via an EPR effect. (Fig. 4B and C). The mice were sacrificed with the collection of

major organs 12 h post-injection, which confirmed that NP_{Ce6} had been metabolised from the liver (Fig. 4D) [43]. The strong luminescence signal recorded in the liver is typically attributed to the metabolic pathway of the NP_{Ce6} *In vivo*. We next evaluated the antitumor performance of NP_{Ce6/Pt} using a subcutaneous 4T1 tumor model. Tumor inhibition effect was quantified by time-dependent tumor volume and tumor weight (Fig. 4E). The control group demonstrated a curve with a rapid growing trend of the tumor volume. Ce6 exhibited a negligible inhibition effect on tumor growth without laser irradiation due to the inexistence of PDT. Encouragingly, NP_{Ce6/Pt} with laser irradiation treated group showed greatly reduced tumor volume. All the tumors were harvested and weighed after 15 days of treatment (Fig. 4G and H). The results are consistent with the tumor growth curves and further confirm the robust therapeutic effects of NP_{Ce6/Pt}. NP_{Ce6/Pt} + -treated group even presented tumor regression and achieved a tumor inhibition rate (TIR) of 93.0 %, demonstrating the excellent synergistic therapeutic effect of PDT and chemotherapy. The enhanced tumor inhibition effect was further assessed by hematoxylin and eosin (H&E) apoptosis evaluation (Fig. 4I and Fig. S16). NP_{Ce6/Pt} + treated group showed apparent tumor cell apoptosis and massive tumour necrosis compared to the control group.

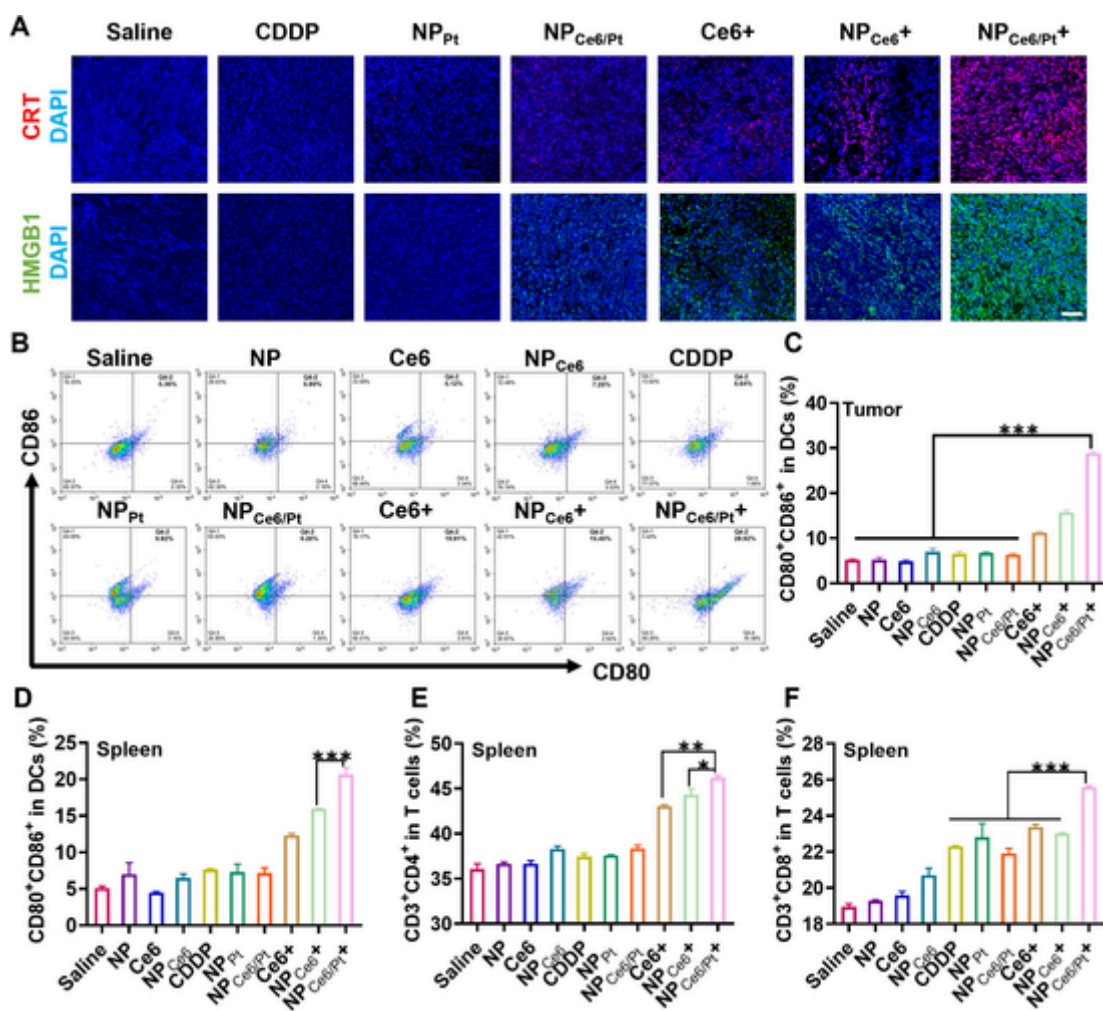


Fig. 5. (A) Immunofluorescence images for the assessment of CRT exposure and HMGB1 release in 4T1 tumors. Scale bar: 100 μm. FCM analyses (B) and quantification (C) of maturation of the DCs (CD11c⁺CD80⁺CD86⁺) in tumor tissues. (D) The percentages of CD80⁺CD86⁺ among total DCs in spleen. (E) The percentage of the CD4⁺ T cells in the spleen following various treatments. (F) The percentage of the CD8⁺ T cells in the spleen following various treatments.

3.5. *In vivo* biosafety study

To further verify the biosafety of nanoparticles *In vivo*, the body weight of mice in each group was monitored and the blood was collected from the mice post-treatment for biochemical analysis. The body weight of mice and serum biochemical index data were both found to remain at acceptable normal levels (Fig. 4F and Fig. S17), implying negligible tissue functional impairment. H&E staining analysis of kidney showed insignificant nephrotoxicity in mice as well (Fig. S18), supporting the excellent biosafety of NP_{Ce6/Pt}.

3.6. *In vivo* antitumor immune response study

The DAMPs release during ICD could be involved in promoting the maturation of DCs and cross-priming of cytotoxic T cells, which subsequently trigger the enhanced immune response [44,45]. To verify the antitumor immune response of NP_{Ce6/Pt} *In vivo*, immunofluorescence staining and FCM analysis were conducted on the tumor and spleen after treatment. The CRT and HMGB1 immunofluorescence analysis in tumor tissues demonstrated that NP_{Ce6/Pt} markedly stimulated CRT and HMGB1 exposure (Fig. 5A) [46]. To further investigate whether NP_{Ce6/Pt} could improve the maturation rate of DCs *In vivo*, FCM analysis on tumor tissues and spleens of mice was conducted. NP_{Ce6/Pt} significantly accelerated DC maturation compared with the saline group leading to significant increases of the splenic and tumor DC maturation

rates was increased from 5.2 % and 5.1 % to 28.8 % and 20.7 %, respectively. (Fig. 5B, C, and D). In addition, considering the crucial role of T cells in immune responses, the changes of the infiltration of CD8⁺ cytotoxic T lymphocytes and CD4⁺ helper T cells in the spleens were identified using flow cytometry. The CD8⁺ and CD4⁺ T cells showed similar trend in spleens (Fig. 5E, F). The CD8⁺ and CD4⁺ T cells barely infiltrated in the spleen when mice were treated with saline. In contrast, the CD8⁺ and CD4⁺ T cells in NP_{Ce6/Pt} group was 1.35-fold and 1.26-fold higher than that in the saline group due to intracellular GSH depletion-enhanced synergistic chemo- and photodynamic therapy. The overall results suggested that NP_{Ce6/Pt} plus laser irradiation efficiently induced ICD and triggered antitumor immunotherapy effects.

4. Conclusions

In summary, we constructed herein a modularized supramolecular nanoplatform by using Azo not only as conjugation sites for molecular integration of multicomponent moieties but also for intracellular GSH depletion-enhanced synergistic chemo- and photodynamic therapy. In addition to inducing tumor cell apoptosis, NP_{Ce6/Pt}-mediated synergistic PDT and chemotherapy promoted CRT exposure, extracellular HMGB1 and ATP leakage for a stronger ICD response, which could further recruit mature DCs and activate CD8⁺ and CD4⁺ T cells for antitumor immune cycles. The NP_{Ce6/Pt} developed herein could act as a promising nanoplatform for enhanced immunogenicity via synergistic

PDT and chemotherapy, which holds great potential for clinical translations.

CRedit authorship contribution statement

Dun Wang : Writing – original draft. **Wei Wang** : Methodology. **Shuang Li** : Methodology. **Hongbin Liu** : Methodology. **Yuqi Zhao** : Methodology. **Dongdong Peng** : Methodology. **Cui-Yun Yu** : Conceptualization, Funding acquisition, Project administration, Writing – review & editing. **Hua Wei** : Conceptualization, Funding acquisition, Project administration, Writing – review & editing.

Declaration of Competing Interest

The authors declare that they have no known competing financial interests or personal relationships that could have appeared to influence the work reported in this paper.

Data availability

Data will be made available on request.

Acknowledgements

The authors acknowledge the financial support from the Thousand Young Talent Program, the Outstanding Youth Fund of Natural Science Foundation of Hunan Province (2017JJ1024), the University of South China Innovation Foundation For Postgraduate (223YXC045), the Foundation of Hunan Provincial Natural Science Foundation of China (2022JJ40381)

Appendix A. Supplementary data

Supplementary data to this article can be found online at <https://doi.org/10.1016/j.cej.2023.143731>.

References

- W. Fan, P. Huang, X. Chen, Overcoming the Achilles' heel of photodynamic therapy, *Chem. Soc. Rev.* 45 (23) (2016) 6488–6519.
- L. Huang, S. Zhao, J. Wu, L. Yu, N. Singh, K. Yang, M. Lan, P. Wang, J.S. Kim, Photodynamic therapy for hypoxic tumors: advances and perspectives, *Coord. Chem. Rev.* 438 (2021) 213888.
- X. Deng, Z. Shao, Y. Zhao, Solutions to the drawbacks of photothermal and photodynamic cancer therapy, *Adv. Sci.* 8 (3) (2021) 2002504.
- K. Sun, J. Hu, X. Meng, Y. Lei, X. Zhang, Z. Lu, L. Zhang, Z. Wang, Reinforcing the induction of immunogenic cell death via artificial engineered cascade bioreactor-enhanced chemo-immunotherapy for optimizing cancer immunotherapy, *Small* 17 (37) (2021) 2101897.
- A.P. Castano, P. Mroz, M.R. Hamblin, Photodynamic therapy and anti-tumour immunity, *Nat. Rev. Cancer* 6 (7) (2006) 535–545.
- S. Zhang, J. Wang, Z. Kong, X. Sun, Z. He, B. Sun, C. Luo, J. Sun, Emerging photodynamic nanotherapeutics for inducing immunogenic cell death and potentiating cancer immunotherapy, *Biomaterials* 282 (2022) 121433.
- X. Li, N. Kwon, T. Guo, Z. Liu, J. Yoon, Innovative strategies for hypoxic-tumor photodynamic therapy, *Angew. Chem. Int. Ed.* 57 (36) (2018) 11522–11531.
- L.-P. Zhao, R.-R. Zheng, H.-Q. Chen, L.-S. Liu, X.-Y. Zhao, H.-H. Liu, X.-Z. Qiu, X.-Y. Yu, H. Cheng, S.-Y. Li, Self-delivery nanomedicine for O₂-economized photodynamic tumor therapy, *Nano Lett.* 20 (3) (2020) 2062–2071.
- S. Xu, X. Zhu, C. Zhang, W. Huang, Y. Zhou, D. Yan, Oxygen and Pt (II) self-generating conjugate for synergistic photo-chemo therapy of hypoxic tumor, *Nat. Commun.* 9 (1) (2018) 2053.
- H. Liu, Y. Hu, Y. Sun, C. Wan, Z. Zhang, X. Dai, Z. Lin, Q. He, Z. Yang, P. Huang, Y. Xiong, J. Cao, X. Chen, Q. Chen, J.F. Lovell, Z. Xu, H. Jin, K. Yang, Co-delivery of bee venom melittin and a photosensitizer with an organic–inorganic hybrid nanocarrier for photodynamic therapy and immunotherapy, *ACS Nano* 13 (11) (2019) 12638–12652.
- G. Yang, S.Z.F. Phua, W.Q. Lim, R. Zhang, L. Feng, G. Liu, H. Wu, A.K. Bindra, D. Jana, Z. Liu, Y. Zhao, A hypoxia-responsive albumin-based nanosystem for deep tumor penetration and excellent therapeutic efficacy, *Adv. Mater.* 31 (25) (2019) 1901513.
- Y. Yang, X. Liu, W. Ma, Q. Xu, G. Chen, Y. Wang, H. Xiao, N. Li, X.-J. Liang, M. Yu, Light-activatable liposomes for repetitive on-demand drug release and immunopotential in hypoxic tumor therapy, *Biomaterials* 265 (2021) 120456.
- W. Zhang, J. Shen, H. Su, G. Mu, J.-H. Sun, C.-P. Tan, X.-J. Liang, L.-N. Ji, Z.-W. Mao, Co-delivery of cisplatin prodrug and chlorin e6 by mesoporous silica nanoparticles for chemo-photodynamic combination therapy to combat drug resistance, *ACS Appl. Mater. Interfaces* 8 (21) (2016) 13332–13340.
- S. Karaosmanoglu, M. Zhou, B. Shi, X. Zhang, G.R. Williams, X. Chen, Carrier-free nanodrugs for safe and effective cancer treatment, *J. Control. Release* 329 (2021) 805–832.
- C. Chen, C. Wu, J. Yu, X. Zhu, Y. Wu, J. Liu, Y. Zhang, Photodynamic-based combinatorial cancer therapy strategies: tuning the properties of nanoplateform according to oncotherapy needs, *Coord. Chem. Rev.* 461 (2022) 214495.
- X. Huang, N. Mu, Y. Ding, H.W. Lam, L. Yue, C. Gao, T. Chen, Z. Yuan, R. Wang, Targeted delivery and enhanced uptake of chemo-photodynamic nanomedicine for melanoma treatment, *Acta Biomater.* 147 (2022) 356–365.
- M. Mohamadoseini, Z. Mohamadnia, Supramolecular self-healing materials via host-guest strategy between cyclodextrin and specific types of guest molecules, *Coord. Chem. Rev.* 432 (2021) 213711.
- J. Wankar, N.G. Kotla, S. Gera, S. Rasala, A. Pandit, Y.A. Rochev, Recent advances in host–guest self-assembled cyclodextrin carriers: Implications for responsive drug delivery and biomedical engineering, *Adv. Funct. Mater.* 30 (44) (2020) 1909049.
- J. Zhu, T. Guo, Z. Wang, Y. Zhao, Triggered azobenzene-based prodrugs and drug delivery systems, *J. Control. Release* 345 (2022) 475–493.
- X.-B. Zhao, W. Ha, K. Gao, Y.-P. Shi, Precisely traceable drug delivery of azoreductase-responsive prodrug for colon targeting via multimodal imaging, *Anal. Chem.* 92 (13) (2020) 9039–9047.
- H.B. Cheng, S. Zhang, J. Qi, X.J. Liang, J. Yoon, Advances in application of azobenzene as a trigger in biomedicine: molecular design and spontaneous assembly, *Adv. Mater.* 33 (26) (2021) 2007290.
- X. Guo, F. Liu, J. Deng, P. Dai, Y. Qin, Z. Li, B. Wang, A. Fan, Z. Wang, Y. Zhao, Electron-accepting micelles deplete reduced nicotinamide adenine dinucleotide phosphate and impair two antioxidant cascades for ferroptosis-induced tumor eradication, *ACS Nano* 14 (11) (2020) 14715–14730.
- J. Wu, Y. Liu, M. Cao, N. Zheng, H. Ma, X. Ye, N. Yang, Z. Liu, W. Liao, L. Sun, Cancer-responsive multifunctional nanoplateform based on peptide self-assembly for highly efficient combined cancer therapy by alleviating hypoxia and improving the immunosuppressive microenvironment, *ACS Appl. Mater. Interfaces* 15 (4) (2023) 5667–5678.
- G. Shu, W. Zhu, Y. Jiang, X. Li, S. Sun, Persistent luminescence immune hydrogel for photodynamic immunotherapy of tumors in vivo, *Adv. Funct. Mater.* (2021).
- H. Xiao, X. Li, B. Li, S. Yang, J. Qin, S. Han, J. Ren, X. Shuai, Nanodrug Inducing Autophagy Inhibition and Mitochondria Dysfunction for Potentiating Tumor Photo-Immunotherapy, *Small n/a(n/a)* 2300280. <https://doi.org/https://doi.org/10.1002/sml.202300280>.
- D. Hu, Y. Deng, F. Jia, Q. Jin, J. Ji, Surface charge switchable supramolecular nanocarriers for nitric oxide synergistic photodynamic eradication of biofilms, *ACS Nano* 14 (1) (2019) 347–359.
- P. Peng, Y. Liu, M. Zhang, F. Liu, L. Ma, C.-Y. Yu, H. Wei, One-pot fabrication of dual-redox sensitive, stabilized supramolecular nanocontainers for potential programmable drug release using a multifunctional cyclodextrin unit, *J. Control. Release* 334 (2021) 290–302.
- Z. Zheng, Z. Guo, F. Zhong, B. Wang, L. Liu, W. Ma, C.-Y. Yu, H. Wei, A dual crosslinked hydrogel-mediated integrated peptides and BMSC therapy for myocardial regeneration, *J. Control. Release* 347 (2022) 127–142.
- Y. Deng, Y. Wang, F. Jia, W. Liu, D. Zhou, Q. Jin, J. Ji, Tailoring supramolecular prodrug nanoassemblies for reactive nitrogen species-potentiated chemotherapy of liver cancer, *ACS Nano* 15 (5) (2021) 8663–8675.
- Z. Xu, C. Pan, W. Yuan, Light-enhanced hypoxia-responsive and azobenzene cleavage-triggered size-shrinkable micelles for synergistic photodynamic therapy and chemotherapy, *Biomater. Sci.* 8 (12) (2020) 3348–3358.
- C. Chen, S. Zhang, R. Zhang, P. Sun, C. Shi, M. Abdalla, A. Li, J. Xu, W. Du, J. Zhang, Y. Liu, C. Tang, Z. Yang, X. Jiang, In situ tuning proangiogenic factor-mediated immunotolerance synergizes the tumoricidal immunity via a hypoxia-triggerable liposomal bio-nanoreactor, *Theranostics* 10 (26) (2020) 11998–12010.
- W. Ma, G.-Y. Kang, L. Sun, C. Meng, Y. Liu, Z. Zheng, M.-C. Jiang, D. Wang, S.H. Pun, C.-Y. Yu, H. Wei, Multicyclic topology-enhanced anticancer drug delivery, *J. Control. Release* 345 (2022) 278–291.
- W. Ma, S. Li, L.-W. Ma, C.-Y. Yu, H. Wei, Multicyclic topology-enhanced micelle stability and pH-sensitivity, *Eur. Polym. J.* 177 (2022) 111446, <https://doi.org/10.1016/j.eurpolymj.2022.111446>.
- R. Barman, R. Bej, P. Dey, S. Ghosh, Cisplatin-conjugated polyurethane capsule for dual drug delivery to a cancer cell, *ACS Appl. Mater. Interfaces* (2023), <https://doi.org/10.1021/acsami.2c22146>.
- J. Ye, B. Yu, H. Hu, D. Zhou, Q. Jin, J. Ji, Z. Tang, Verteporfin-loaded supramolecular micelles for enhanced cisplatin-based chemotherapy via autophagy inhibition, *J. Mater. Chem. B* 10 (14) (2022) 2670–2679.
- G.-G. Yang, Z.-Y. Pan, D.-Y. Zhang, Q. Cao, L.-N. Ji, Z.-W. Mao, Precisely assembled nanoparticles against cisplatin resistance via cancer-specific targeting of mitochondria and imaging-guided chemo-photothermal therapy, *ACS Appl. Mater. Interfaces* 12 (39) (2020) 43444–43455.
- C. Chu, X. Lyu, Z. Wang, H. Jin, S. Lu, D. Xing, X. Hu, Cocktail polyprodrug nanoparticles concurrently release cisplatin and peroxynitrite-generating nitric oxide in cisplatin-resistant cancers, *Chem. Eng. J.* 402 (2020) 126125.
- Y. Li, L. Lin, J. Xie, L. Wei, S. Xiong, K. Yu, B. Zhang, S. Wang, Z. Li, Y. Tang, G. Chen, Z. Li, Z. Yu, X. Wang, ROS-triggered self-assembled nanoparticles based on a chemo-sonodynamic combinational therapy strategy for the noninvasive elimination of hypoxic tumors, *ACS Appl. Mater. Interfaces* 15 (12) (2023)

- 15893–15906.
- [39] Y. Liu, D. Wang, H. Liu, L. Liu, S. Li, Z. Zhou, L. Lu, X. Liu, L. He, D. He, C.-Y. Yu, H. Wei, A clinically translatable ternary platinum (IV) prodrug for synergistically reversing drug resistance, *J. Med. Chem.* 66 (6) (2023) 4045–4058.
- [40] E.M. Kosower, H. Kanety-Londner, Glutathione. 13. Mechanism of thiol oxidation by diazenedicarboxylic acid derivatives, *J. Am. Chem. Soc.* 98 (10) (1976) 3001–3007.
- [41] Y. Chen, T. Xiong, X. Zhao, J. Du, W. Sun, J. Fan, X. Peng, Tumor cell-responsive photodynamic immunoagent for immunogenicity-enhanced orthotopic and remote tumor therapy, *Adv. Healthc. Mater.* 12 (5) (2023) 2202085.
- [42] D. Wei, Y. Chen, Y. Huang, P. Li, Y. Zhao, X. Zhang, J. Wan, X. Yin, T. Liu, J. Yin, NIR-light triggered dual-cascade targeting core-shell nanoparticles enhanced photodynamic therapy and immunotherapy, *Nano Today* 41 (2021) 101288.
- [43] J. Wang, J.-J. Nie, P. Guo, Z. Yan, B. Yu, W. Bu, Rhodium (I) complex-based polymeric nanomicelles in water exhibiting coexistent near-infrared phosphorescence imaging and anticancer activity *In vivo*, *J. Am. Chem. Soc.* 142 (6) (2020) 2709–2714.
- [44] G. Kroemer, C. Galassi, L. Zitvogel, L. Galluzzi, Immunogenic cell stress and death, *Nat. Immunol.* 23 (4) (2022) 487–500.
- [45] X. Qin, M. Zhang, Z. Zhao, Q. Du, Q. Li, Y. Jiang, F. Xue, Y. Luan, A carrier-free photodynamic nanodrug to enable regulation of dendritic cells for boosting cancer immunotherapy, *Acta Biomater.* 147 (2022) 366–376.
- [46] H. Deng, Z. Zhou, W. Yang, L.-S. Lin, S. Wang, G. Niu, J. Song, X. Chen, Endoplasmic reticulum targeting to amplify immunogenic cell death for cancer immunotherapy, *Nano Lett.* 20 (3) (2020) 1928–1933.

CORRECTED PROOF